ARTICLE
Traditional Medicine Research 2023;8(8):45. https://doi.org/10.53388/TMR20230117001

Effect of salvianolic acid B-loaded mesoporous silica nanoparticles on myocardial ischemia-reperfusion injury

Ming-Juan Yang[1#], Xiao-Ying Han[1#], Ou Qiao[1], Hai-Xia Ji[1], Yi Zhang[1], Xin-Yu Zhang[1], Wen-Zhe Wang[1], Xia Li[1], Juan Wang[1], Lan-Ping Guo[2], Lu-Qi Huang[2], Wen-Yuan Gao[1*]

[1]School of Pharmaceutical Science and Technology, Tianjin University, Tianjin 300072, China. [2]National Resource Center for Chinese Materia Medica, China Academy of Chinese Medical Sciences, Beijing 100700, China.

[#]Ming-Juan Yang and Xiao-Ying Han are the co-first authors of this paper.

[*]**Corresponding to:** Wen-Yuan Gao, Tianjin Key Laboratory for Modern Drug Delivery and High Efficiency, School of Pharmaceutical Science and Technology, Tianjin University, No. 92, Weijin Road, Nankai District, Tianjin 300072, China. E-mail: pharmgao@tju.edu.cn.

Author contributions

Yang MJ and Han XY designed this study, conceived this study, carried out this study, analyzed the data and drafted the manuscript. Qiao O designed the study, collected and analyzed the data. Ji HX, Zhang XY, Zhang Y and Wang WZ investigated the study. Li X and Wang J were responsible for this manuscript and reviewed the article critically. Guo LP and Huang LQ helped accomplish the conception and design of the study. Gao WY provided technical consulting and material support. All authors read and approved the final manuscript.

Competing interests

The authors declare no conflicts of interest.

Acknowledgments

We acknowledge the teachers from the Institute of Radiation Medicine, Chinese Academy of Medical Sciences for the I/R help in animal experiments.

Peer review information

Traditional Medicine Research thanks all anonymous reviewers for their contribution to the peer review of this paper.

Abbreviations

SalB, salvianolic acid B; MSNs, mesoporous silica nanoparticles; RhB, rhodamine B; PBS, phosphate-buffered saline; H/R, hypoxia/reoxygenation; PI, propidium iodide; I/R, ischemia-reperfusion; TUNEL, terminal deoxynucleotidyl transferase-mediated dUTP-biotin nick end labeling; HE, hematoxylin-eosin staining; LV, left-ventricular; ROS, reactive oxygen species.

Citation

Yang MJ, Han XY, Qiao O, et al. Effect of salvianolic acid B-loaded mesoporous silica nanoparticles on myocardial ischemia-reperfusion injury. *Tradit Med Res*. 2023;8(8):45. doi: 10.53388/TMR20230117001.

Executive editor: Xin-Yi Yang.

Received: 17 January 2023; **Accepted:** 15 March 2023; **Available online:** 29 March 2023.

Abstract

Background: Currently, no drugs can specifically improve clinical cardiac ischemia-reperfusion injury or the prognosis of hemodialysis. Salvianolic acid B (SalB) is a widely used cardiac protectant; however, its clinical application is limited by its low oral bioavailability and poor intestinal absorption. The exploration of its preparation and clinical applications has become a research hotspot in recent years. **Methods:** To determine whether mesoporous silica nanoparticles (MSNs) efficiently delivered SalB to the heart and SalB@MSNs-RhB reduced myocardial ischemia-reperfusion injury, we constructed a myocardial ischemia-reperfusion male rat model, hypoxia/reoxygenation cardiomyocytes, and treated them with SalB@MSNs-RhB. **Results:** SalB@MSNs-RhB showed improved bioavailability, therapeutic effect, heightened JAK2/STAT3-dependent pro-survival signaling, and antioxidant responses, thereby protecting cardiomyocytes from ischemia-reperfusion injury-induced oxidative stress and apoptosis. **Conclusion:** This use of SalB-loaded nanoparticles and investigation of their mechanism of action may provide a new strategy for treating cardiomyocytes. Thus, hypoxia/reoxygenation promotes the clinical application of SalB.

Keywords: salvianolic acid B; myocardial ischemia-reperfusion injury; mesoporous silica; nanoparticles

Highlights

1. The use of salvianolic acid B (SalB)-loaded nanoparticles and the exploration of the mechanism of action may provide a new strategy for the treatment of cardiomyocyte hypoxia/reoxygenation.
2. SalB and SalB@mesoporous silica nanoparticles-rhodamine B have defensive effects on cardiacfunction in rats with myocardial ischemia-reperfusion injury and their mechanisms of action may be bassociated with the reduction of oxidative stress and inhibition of cellular regulation.
3. SalB@mesoporous silica nanoparticles-rhodamine B can improve the bioavailability and therapeutic effects of SalB, heighten JAK2/STAT3-dependent pro-survival signaling and antioxidant responses.

Background

Heart is the key organ of the cardiovascular system, that ensures blood flow in the blood vessels such that body tissues receive sufficient nutrients, oxygen, and other components. Myocardial ischemia is a common disease caused by an imbalance between the provisioning and demand of arterial circulation and myocardial cells, with a complex pathogenesis and high mortality, affecting the quality of life in patients [1]. Treatment methods for coronary artery stenosis or blockage, such as urokinase thrombolytic and percutaneous coronary intervention are used to remove it and restore myocardial blood supply [2]. Myocardial cell reperfusion after a period of ischemia results in varying degrees of myocardial tissue damage, known as myocardial ischemia/reperfusion injury [3–5]. In recent years, the alleviation of myocardial ischemia-reperfusion (I/R) injury has become a crucial challenge to be addressed. In Western medicine, drugs are typically synthesized chemically or from natural products, involving organic and inorganic chemistry and biology. Western medicine plays a very important role in the treatment of diseases. However, application of western medicine resulted in various side effects, including gastrointestinal reactions and liver, kidney, and vision damage. These drugs have serious impacts on patients, their recovery, and medical expenses [6]. While Western medicine shows sufficient curative effect in treating myocardial ischemia, its use is limited by the side effects caused, creating a dilemma regarding its use among patients and doctors. Many traditional Chinese medicine prescriptions actively prevent and treat myocardial I/R injury.

The *Salviae Miltiorrhizae Radix et Rhizoma* (Danshen) is the most abundant source of salvianolic acid. It has been widely used to treat cardiovascular diseases [7]. Salvianolic acid B (SalB) is the key active compound in the pharmacology of salvianolic acid providing significant cardiovascular protection [7, 8]. SalB is the main effective water-soluble component of the salvianolic base, inhibiting blood platelet aggregation and thrombosis [9]. SalB exhibits biological activities such as anti-lipid peroxidation, anti-liver fibrosis, anti-atherosclerosis, free radical scavenging, calcium antagonism, and improvement of memory dysfunction [10–12]. It also exhibits cardio-protective effects in experimental animals with myocardial cell injury by promoting angiogenesis [13].

Although SalB is a widely used cardioprotective agent, its clinical application is limited due to its low oral bioavailability and poor intestinal absorption [14].

Nanocarriers can significantly improve the bioavailability and pharmacokinetics of compounds, thereby improving the treatment efficacy of SalB [15–17]. Compared to traditional drugs, the size, shape and material properties of nanomedicine, effectively improves their therapeutic effect and reduces side effects by enhancing pharmacokinetic and pharmacodynamic properties [18]. In this context, mesoporous silica particles have properties that improve drug dissolution, including high surface area, large pore volume, and long-range ordered pore structures [19]. Mesoporous silica nanoparticle (MSN) are promising drug carriers, with various types of small or large molecule drugs, such as ibuprofen, aspirin, biotin-antibiotin protein, and alendronic acid sodium, being loaded into it for application[20]. MSN have a large surface area, a high drug-loading capacity, improved thermal stability and biocompatibility than other materials. Since silica does not accumulate in the body, it degrades, and its degradation products are excreted through the kidneys [21–23]. MSN can be loaded with many drug molecules with high-quality slow-release properties, Therefore, MSN were used in our experiments.

A is associated with rhodamine B (RhB) [24]. This fluorescent dye, created by M. Cérésole in 1888 under the name tetraethyl rhodamine, has been widely used in biology and biotechnology for more than a century [25]. MSN-RhB was synthesized using RhB in this study.

In this study, mesoporous silica materials were prepared for loading SalB, to improve its stability and bioavailability. We constructed rat ischemia reperfusion and rat cardiomyocyte hypoxia/reoxygenation (H/R) models to explore the underlying molecular mechanisms of ischemic reperfusion.

The use of SalB-loaded nanoparticles and investigating their mechanism of action may provide a new strategy for treating of cardiomyocyte H/R, thereby promoting the clinical application of SalB.

Materials and methods

Materials

We purchased butanol, acetic acid, and hydrochloric acid from Anedra Co., Ltd. (Buenos Aires, Argentina), and SalB from Macklin (98.52% purity). Results Pluronic P123 was obtained from Sigma-Aldrich Trading Co.，Ltd. (Shanghai, China), tetraethyl orthosilicate (MW = 208.33), RhB (MW = 479.01) and 3-aminopropyl-triethoxysilane were purchased from Meryer (Shenzhen, China). Spectral grade potassium bromide was purchased from Merck (Darmstadt, Germany). The reagents are analytical grade and are used exactly as they are received from the supplier.

Synthesis and characterization of mesoporous silica nanoparticles-rhodamine B (MSNs-RhB)

P123 was dissolved in 40 ˚C hydrochloric acid. Synthetic silane coupling agents of TEOS and RhB (RhB-aminopropyl-triethoxysilane) were added to the mixed solution at a 10,000 to 1 molar ratio and stirred strongly for 24 hours under photoseal conditions. The red synthetic material was collected by centrifugation. The synthesized material was extracted several times with 150 mL mixture of ethanol and 2 mL 36–38% hydrochloric acid to completely remove the surfactant. The final product MSNs-RhB was vacuum dried overnight at 80 ˚C and then stored in cool, dry and photosealed conditions.

The N_2 adsorption-desorption isotherms were determined by brunauer-Emmet-Teller multi-point method and an analysis of the materials' specific surface area was conducted. An Autosorb iQ Gas adsorption analyzer (Quantachrome Instruments) was used to perform the analysis. A seven-hour degassing and drying procedure was performed before analysis of MSNs-RhB. The pore size distribution was acquired using Barrett-Joyner-Halenda model. Parameters were measured by dynamic light scattering (Malvern Zetasizer Nano-ZS) to value MSNs-RhB particle size, polydispersion index and Zeta potential.

Synthesis and characterization of SalB@MSNs-RhB

First, MSNS-RhB was dried in a vacuum at 100 ˚C for 24 hours, then continuing to be hold on in vacuum at 25 ˚C for 3 hours. Then 5 mg SalB was then completely dissolved in 10 mL anhydrous ethanol and refrigerated at −20 ˚C for 30 min. The ethanol solution of SalB (2–3 drops) is added drop by drop to the dried MSN-RhB until completely soaked. The soaked SalB@MSNs-RhB is then slowly vacuumized at room temperature for half-hour. Repeat the mark-vacuum procedure until 10 mL of SalB ethanol solution is used up. Finally, the prepared SalB@MSNs-RhB was sealed in an exceedingly brown bottle and hold on at −20 ˚C.

With dynamic light scattering, we measured SalB@MSNs-RhB's zeta potential and particle size related parameters. The morphology of SalB@MSNs-RhB was observed under accelerated voltage By scanning electron microscopy (LEO1530VP, Carl Zeiss AG CO., Ltd., Oberkochen, Germany), as well as transmission electron microscopy (JEM2100, JEOL (BEIJING) CO., Ltd., Beijing, China).

Pure compound (SalB), material (MSNS-RhB) and SalB loaded nanoparticles (SalB@MSNs-RhB) were characterized by Fourier transform infrared spectroscopy (FT-IR) (Tensor 27, Bruker, Ettlingen, Germany). The specimen was mixed with KBr to obtain I/R spectra between 400 and 4000 cm^{-1}(mean scan = 64, resolution = 4 cm^{-1}).

In vitro drug release of SalB@MSNs-RhB and in vivo biodistribution

In vitro release assays were performed using dialysis in phosphate-buffered saline (PBS, pH 7.4) at 37 °C. The sealed dialysis bags were put into brown bottles and shaken on a constant temperature shaker under dark conditions. After being shaken well, the supernatant was collected by centrifugation for 0 h, 2 h, 5 h, 10 h, 15 h, 20 h, 30 h, 50 h, 70 h, 100 h and 120 h. The absorbance at 284 nm was measured by UV spectrophotometer, the concentration of SalB in supernatant was calculated according to Lambert Beer's law, and the release curve of SalB in vitro was plotted on it.

There were two groups of 12 Sprague Dawley rats each, randomLy divided. After SalB and SalB@MSNs-RhB were administered respectively, the abdominal aorta was collected at 0 min, 5 min, 10 min, 20 min, 40 min, 80 min, 100 min, 120 min, 180 min, 240 min, 300 min, and 360 min for bioavailability analysis.

Myocardial cell model of I/R

Cells from Chinese Academy of Science (Shanghai, China) were used for this study and cultured in Dulbecco's Modified Eagle's Medium high glucose medium (Sigma-Aldrich, Madison, WI, USA) + 10% FBS (Sigma-Aldrich) + 1% double antibodies (Gibco, Grand Island, NY, USA) as the medium, in the incubator (5% CO_2) (MCO-5AC, Panasonic, Kyoto, Japan) at 37 °C.

Four groups of myocardial cells were studied: control, H/R, SalB, and SalB@MSNs-RhB. When H/R group cells grew close to fusion state in the incubation process of 5% CO_2 and 37 °C, they were placed in a hypoxia chamber containing 95% N_2 and 5% CO_2 mixture to simulate the hypoxia environment. The hypoxic chamber was placed at 37 °C to maintain 95% N_2 equilibrium and 5% CO_2 hypoxia for 3 h. Then, the cells were transferred from anoxic chamber condition to normal cell culture condition (95% O_2, 5% CO_2, 37 °C) to simulate reperfusion and reoxygenation for 2 h. Control cells were cultured at 37°C with 5% CO2 without H/R. SalB group and SalB@MSNs-RhB group were treated with SalB and SalB@MSNs-RhB (10 μM, 20 μM, 40 μM and 80 μM) for 24 h, and then an h/R damage step was done.

Cell viability and apoptosis

1×10^4 cells/well cells were cultured in 96-well plates. After 24 hours, cells were washed in PBS and treated with SalB@MSNs-RhB and SalB at different concentrations (10–80 μM) for 24 h. Cellular activity was detected with the cell counting kit-8. Afterwards, the viability of the cells was evaluated using the cell counting kit-8, according to the manufacturer's instructions. We added 10 μL of CCK8 solution to each well, and the specimens were incubated for two hours at 37 °C before measuring the I/R absorbance at 450 nm. Following that, the absorbance was measured at 450 nm. At least six experiments were conducted for each sample.

Apoptosis detection is performed using flow cytometry, using an annexin V/PI apoptosis detection kit purchased from Dalian Meilun Biological Co., Ltd. (Dalian, China). A combination of annexin V (AV)-fluorescein isothiocyanate and propidium iodide (PI) was used to differentiate apoptotic cells from living or dying cells. The cells were washed double, and also the concentration was adjusted to 1×10^6 cells /mL with a chilly buffer. Incubated at 25 °C, room temperature, dark for fifteen minutes with 10 μL AV-fluorescein isothiocyanate and 10 μL PI each. Incubation with the two reagents was carried out separately for 15 min under dark conditions and flow analysis was performed with the binding buffer. Finally, 400 μL binding buffer was added to every specimen without washing and flow cytometry was used for analysis.

First, the cover glass was placed into the 24-well cell culture plate, and then the cells were inoculated on the cover glass of the 24-well cell culture plate for 24 hours. After the slides were completed, each well was fixed with 500 μL paraformaldehyde at 4 °C for 30–40 min at room temperature. After washing with PBS, cells were incubated with 10 μg/mL Hoechst at 37 °C for 7 minutes. After cultivation with Hoechst 33342, the cells were incubated with PI (2.5 μg/mL). Leave the culture plate in the dark for 15 minutes. Cells were washed with PBS after cultivation and instantly observed under an inverted fluorescence microscope (Nikon Co., Ltd., Shanghai, China).

Animal model and drug administration

Sprague-Dawley male rats (180–200 g, SCXK-2019-0010) were provided by Beijing HFK Biotechnology Co., Ltd. (Beijing, China). The rats got one week to regulate to the new setting before the experiments. All rats were fed in rat cages, 5 rats per box, placed on laminar flow racks to ensure a well-ventilated, noise-free animal room with an ambient temperature of 22 °C ± 1 °C, relative humidity of 50% ± 10%, 12 hours of light/dark cycles (8 am–8 pm), and free food and water. Control, I/R and drug treatment groups were randomly assigned. For the I/R model, rats were anesthetized using isoflurane I/R anesthesia, an open thoracotomy was performed next to the left sternum at the fifth intercostal space, and the pericardium was completely exposed. Left coronary artery was inserted between left atrial appendage and pulmonary artery. With 6-0 silk thread, the anterior descendent branch of the left coronary artery was ligated. After 1 hour, the sutures were detached for reperfusion. The specific operation was shown in Figure 1. The operation is successful when the color of the distal anterior wall of the ligation turns purple and the ST segments of leads I, II and a high and left lateral lead increase by 0.2 m as determined by the electrocardiogram monitoring.

In the experiment, four groups of rats were randomly divided. These were the control group, the group receiving I/R, the SalB group, and the SalB@MSNs-RhB group. I/R was not administered to control rats.

Normal saline was administered to rats in the I/R group for 10 days prior to I/R, and SalB (80 μmol/L) and SalB@MSNs-RhB (80 μmol/L) groups were given ingastric administration for 10 days before I/R. The rats were injected intravenously with SalB or SalB@MSNs-RhB at a dose of 5 mg/kg. The procedures were conducted in accordance with "Guiding Principles for the Care and Use of Animals" and approved by Tianjin Medical University's Institutional Animal Care and Use Committee (SYXK-2014-0002).

Echocardiographic assessment of left ventricular function

Anesthesia was administered to the rats with pentobarbital sodium (0.2 mL/100 g) after modeling and left-ventricular (LV) function was assessed using Vevo 2100 (VisualSonic, Toronto, Canada) ultra-high resolution animal ultrasound imaging system. Evaluate the following parameters as functional indicators: Systolic ventricular septum, diastolic ventricular septum, left ventricular systolic diameter, left ventricular diastolic diameter, ejection fraction, shortened fraction and so on.

Histopathological and immunofluorescence analysis of the heart

At the end of the experiment, the heart was quickly detached and fixed in 4% paraformaldehyde solution. The heart wax block was prepared by conventional dewatering and wax rewaxing procedure and cut into thin slices. Routine hematoxylin-eosin staining (HE) staining technique was accustomed to observe the morphology of cardiac fibrosis in every group under light microscope. The immovable heart sections were measured with the terminal deoxynucleotidyl transferase-mediated dUTP-biotin nick end labeling (TUNEL) assay kit (Roche) in step with the manufacturer's N-dipropylacetate/Rections. After staining the nuclei with 4',6-diamidino-2-phenylindole, the TUNEL assay was performed.

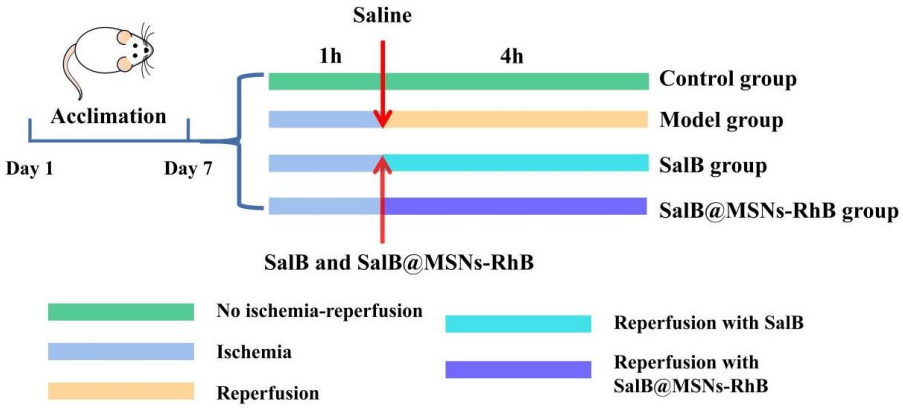

Figure 1 Schematic illustration of I/R model and treatment. SalB, salvianolic acid B; MSNs, mesoporous silica nanoparticles; RhB, rhodamine B; I/R, ischemia-reperfusion.

Apoptosis in rat myocardial tissue determined by TUNEL staining.

Biochemical analysis

Rats in each group had the I/R arterial blood collected and kept at room temperature 30 minutes before undergoing the study. Serum separation was done via spinning at 4,000 rpm for 10 min. It was tested using a kit (Shanghai FANKEL Industrial Co., Ltd., (Shanghai, China) for enzyme immunoassay to measure the content changes of creatine kinase isoenzyme-MB, superoxide dismutase, malondialdehyde, aspartate transaminase, alanine aminotransferase and caspase-3 in the serum according to the manufacturing scheme.

Western blot analysis

By Western blotting, we examined the expression of proteins belonging to the JAK signaling pathway (JAK2 and STAT3) and related to apoptosis (caspase-3, Bax, and Bcl-2). The heart tissue (100 mg) was incubated in 1 mL RIPA buffer (1% sodium deoxycholate, 1% Triton X-100, 0.1% SDS, 15 mM HEPES NaOH (pH 7.5), 10 mM EDTA, 0.15 mM NaCl, 1 mM sodium orthovanadate, and 0.5% protease inhibitor mixture (Sigma Chemical Co., Ltd., Louis, MO, USA)) and centrifuged at 12,000 rpm for 5 min at less than 4 °C. The protein (100 μg) sodium dodecyl sulfate polyacrylamide gel electrophoresis was resolved on sodium dodecyl sulfate polyacrylamide gel electrophoresis gel 15% and transferred onto a PVDF membrane (Millipore Co., Ltd., Shanghai, China) Cat#ISEQ00010). Each membrane was sealed with 5% skimmed milk powder in Tris buffered saline (TBS), and detected with anti-beta actin polyclonal (1:4000, PTG 20536-1-AP), anti-Bcl2 antibody (1:1000, BosterBA0290), anti-Bax antibody (1:1000, Boster/BM4624), anti-Caspase3 (1:1000, Boster A01517-2), anti-JAK2 antibody (1:200, Boster/BA3379), anti-STAT3 antibody (1:1000, Boster/BA3379).

Following this, the second antibody conjugated with horseradish peroxidase was incubated according to the manufacture's instructions. The blotted proteins were examined and quantified using an Odyssey Infrared Imaging System (LI-COR, Lincoln, NE, USA). β-Actin was used as an internal control.

Statistical analysis

All data are in mean ± Sprague Dawley format. An analysis of variance was conducted using the one-way analysis of variance method, followed by a Turkeys test for post-hoc analyses. This study was statistically significant when $P < 0.05$ was considered. Statistical computations were conducted with the software GraphPad Prism 9. Statistical computations included $*P < 0.05$, $**P < 0.01$, $***P < 0.001$, **** $P < 0.0001$.

Results

Synthesis and characterization of MSNs-RhB

The synthesized loading material is shown in Figure 2A as a solid pink powder. The particle size distribution of freshly prepared MSNs-RhB is shown in Figure 2B. The average particle size of MSNs-RhB was 123 ± 3.28 nm, and its poly-dispersion index was 0.35, indicating that the particle size distribution was narrow and unimodal. MSNs-RhB had a classic type IV nitrogen adsorption-desorption isotherm at a relative pressure of 0.4–0.8 (P/P0) (Figure 2C, 2D). The average pore size of MSNs-RhB was 8.5 nm, indicating that MSNs-RhB had a uniform mesoporous channel and a relatively narrow pore size distribution. In addition, zeta potentials of MSNs-RhB and SalB were 26.9 ± 5.8 mV and −9.68 ± 2.8 mV, respectively (Figure 2E, 2F). This indicated that MSNs-RhB were positively charged to a large extent by the RhB groups covalently grafted onto the mesoporous channel. This positive charge of MSNs-RhB was expected to pull negatively charged SalB from the polar media into the I/R mesoporous channels via electrostatic attraction or hydrogen bonding. Due to this electrostatic attraction, SalB molecules (ions) were expected to be released from the constructed SalB@MSNs-RhB in a sustained manner.

Characterization of SalB@MSNs-RhB

The physical structural parameters of SalB@MSNs-RhB nanoparticles and their I/R release behaviors in vitro and in vivo were characterized. The prepared SalB@MSNs-RhB are shown in Figure 3A. The damped-least-squares method was used to characterize the particle size (Figure 3B). The SalB@MSNs-RhB had an average diameter of 110 nm. The scanning electron microscopy and transmission electron microscopy results showed that SalB@MSNs-RhB had a spherical shape, with uniform particle size of approximately 110 nm and were highly dispersed (Figure 3C, 3D). The in vitro drug release behavior of SalB and SalB@MSNs-RhB in each group is shown in Figure 3E. A typical cumulative release curve was generated to compare the two releases. The results showed that the release duration exceeded 120 h for SalB@MSNs-RhB, , and there was no evidence of an initial burst release. In contrast, SalB exhibited stagnating release characteristics, releasing only 30–32% of SalB at its endpoint.

To accurately determine whether SalB was successfully loaded onto MSN-RhB, FT-IR was performed. The FT-IR spectrum revealed common bands of pure SalB (Figure 3F). The peak at 3,369 cm^{-1} was caused by the stretching vibration of the -OH group in SalB, and the peaks at 1,113 cm^{-1}, 1,369 cm^{-1} were attributed to the stretching vibration of the -C = O group. The chemical properties of the MSN-RhB carriers were confirmed by FT-IR spectroscopy. The absorption band near 3,739 cm^{-1} exhibited a symmetric stretching vibration pattern of the OH bonds associated with the silanol (Si-OH) group. The peaks at 1,093 cm^{-1} and 962 cm^{-1} were caused by the antisymmetric vibration of the non-bonded oxygen atom (Si-O) of Si-OH and symmetric stretching vibration of the Si-O-Si group, respectively. In MSNs-RhB, an internal vibration peak was observed near 467 cm^{-1} between the Si and O–Si tetrahedrons. In addition, a typical band associated with the stretching vibration of the Si-OH

group appeared at 802 cm^{-1}. After loading, FT-IR spectrum showed typical MSNs-RhB band (at 1,080 cm^{-1}), indicating that the material's surface chemical properties remained unchanged. In addition, FT-IR spectra revealed the presence of SalB in the mesoporous carriers. At the same dose, the SalB concentration in the plasma of SalB@MSNs-RhB-treated rats was consistently higher than that in the SalB-treated group (Figures 3G). The area under the curve [AUC (0-t)] of SalB@MSNs-RhB (2,612 μg/mL•min) was 2.42 times higher than that of SalB (1,080 μg/mL•min). Thus, SalB@MSNs-RhB were more effective in improving the bioavailability of SalB.

Determination of cell activity and apoptosis

Figures 4A shows the effect of SalB@MSNs-RhB on the cellular status of cardiomyocytes. H9C2 cell activity decreased significantly after H/R injury. The addition of SalB@MSNs-RhB had no significant effect on the normal myocardial cell status.

In this study, myocardial cells were induced by H/R to construct an I/R model, and apoptosis was observed through Annexin V/PI staining and Hoechst/PI double staining. Both SalB and SalB@MSNs-RhB inhibited cell apoptosis (Figures 4B, 4C). In contrast, the inhibitory effect of SalB@MSNs-RhB was stronger than that of SalB. As well as

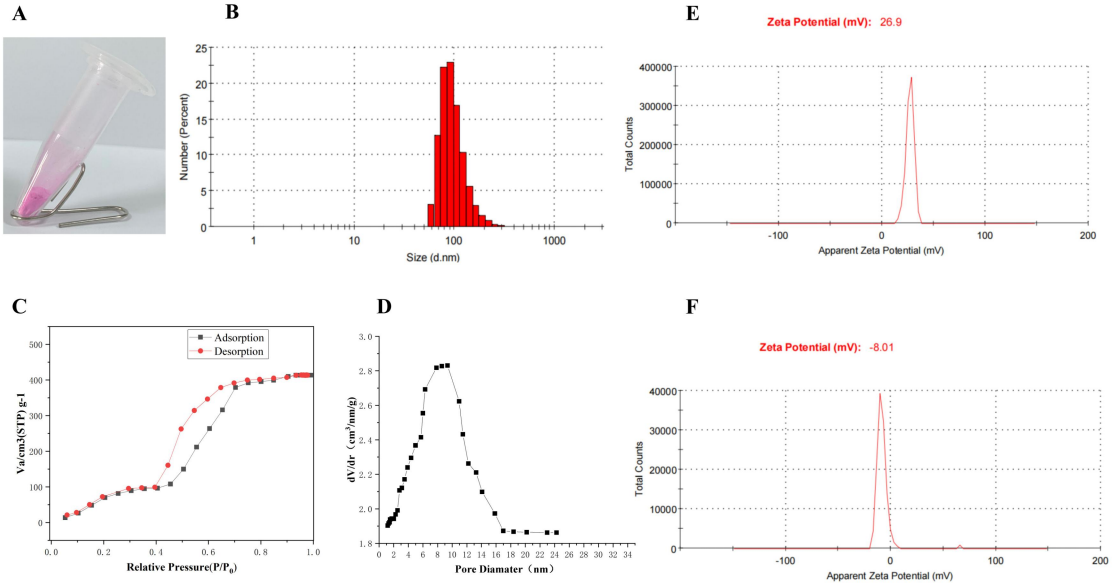

Figure 2 Characterization of MSNs-RhB. (A)Physical appearance of MSNs-RhB. (B) Particle size characterization of MSNs-RhB. The particle size was about 123 nm. (C) N2 adsorption-desorption isotherms of MSNs-RhB. (D) The pore size distribution of MSNs-RhB. (E) Zeta Potential characterization of MSNs-RhB. (F) Zeta Potential characterization of SalB. MSNs, mesoporous silica nanoparticles; RhB, rhodamine B.

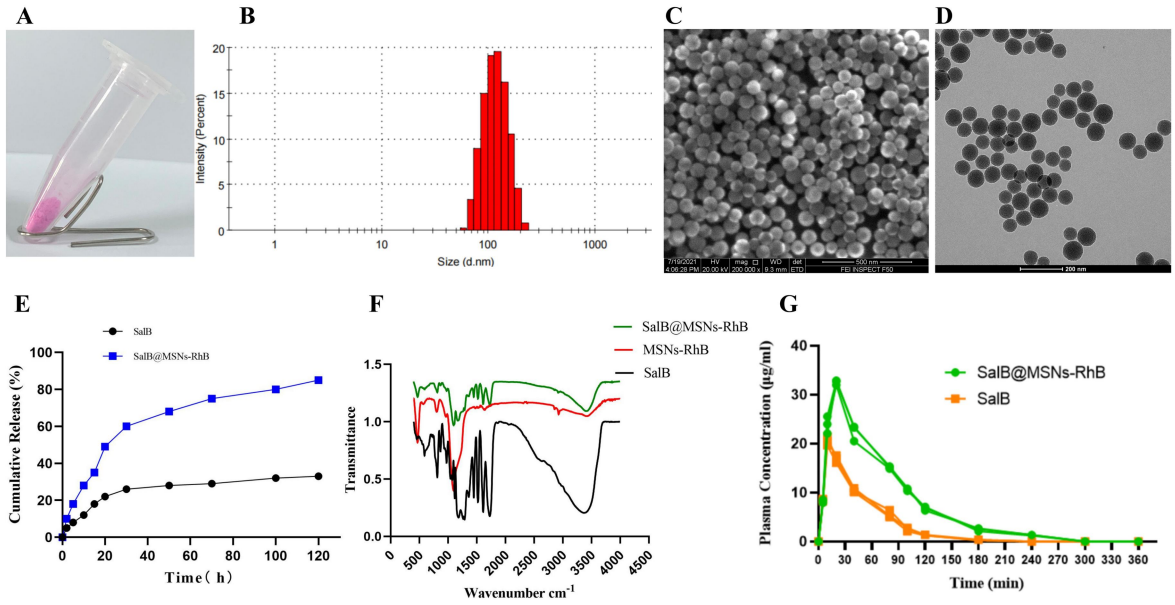

Figure 3 Physical structural parameters of SalB@MSNs-RhB nanoparticles and characterization of I/R in vitro release behavior. (A) Appearance of SalB@MSNs-RhB. (B) Particle size characterization of SalB@MSNs-RhB. The particle size was about 110 nm. (C) SEM image of SalB@MSNs-RhB, with a scale of 500 nm. (D) TEM image of SalB@MSNs-RhB, with a scale of 200 nm. (E) In vitro SalB release kinetics of SalB@MSNs-RhB over 120 h. (F) FT-IR spectra of SalB@MSNs-RhB and MSNs-RhB. (G) SalB@MSNs-RhB nanoparticles and SalB concentrations in plasma (n = 5). SalB, salvianolic acid B; MSNs, mesoporous silica nanoparticles; RhB, rhodamine B; SEM, scanning electron microscope; TEM, transmission electron microscopy.

to those in the normal group after SalB@MSNs-RhB (Figures 4D, 4E). Hoechst33342 uses krypton laser to excite ultraviolet light at excitation and emission wavelengths of 352 nm and 400–500 nm, respectively, producing blue fluorescence. PI uses an argon-ion laser to generate fluorescence. The excitation wavelength was 488 nm, and the emission wavelength was greater than 630 nm, producing red fluorescence. The normal living cells were resistant to the dye and exhibited reduced blue and red fluorescence. Apoptotic cells showed changes in membrane permeability, mainly due to the ingestion of Hoechst dye, showing strong blue fluorescence. Necrotic cells showed strong red fluorescence from strong PI staining. The blue and red fluorescence were strong in the model group (Figure 5), with the number of apoptotic and necrotic cells increasing significantly ($P < 0.05$). Compared to the model group, blue and red fluorescence decreased in the SalB and SalB@MSNs-RhB groups, which had inhibitory effects on cell apoptosis and necrosis. Compared to the SalB group, the SalB@MSNs-RhB group had a stronger inhibitory effect.

Echocardiography and HE staining

As shown in Figure 6, the non-invasive method of echocardiography was used to assess cardiac function after I/R. In the model group, EF and FS were significantly reduced than in the control group. Based on this result, it was concluded that the cardiac function in the model group was significantly impaired/red. This indicated that the I/R

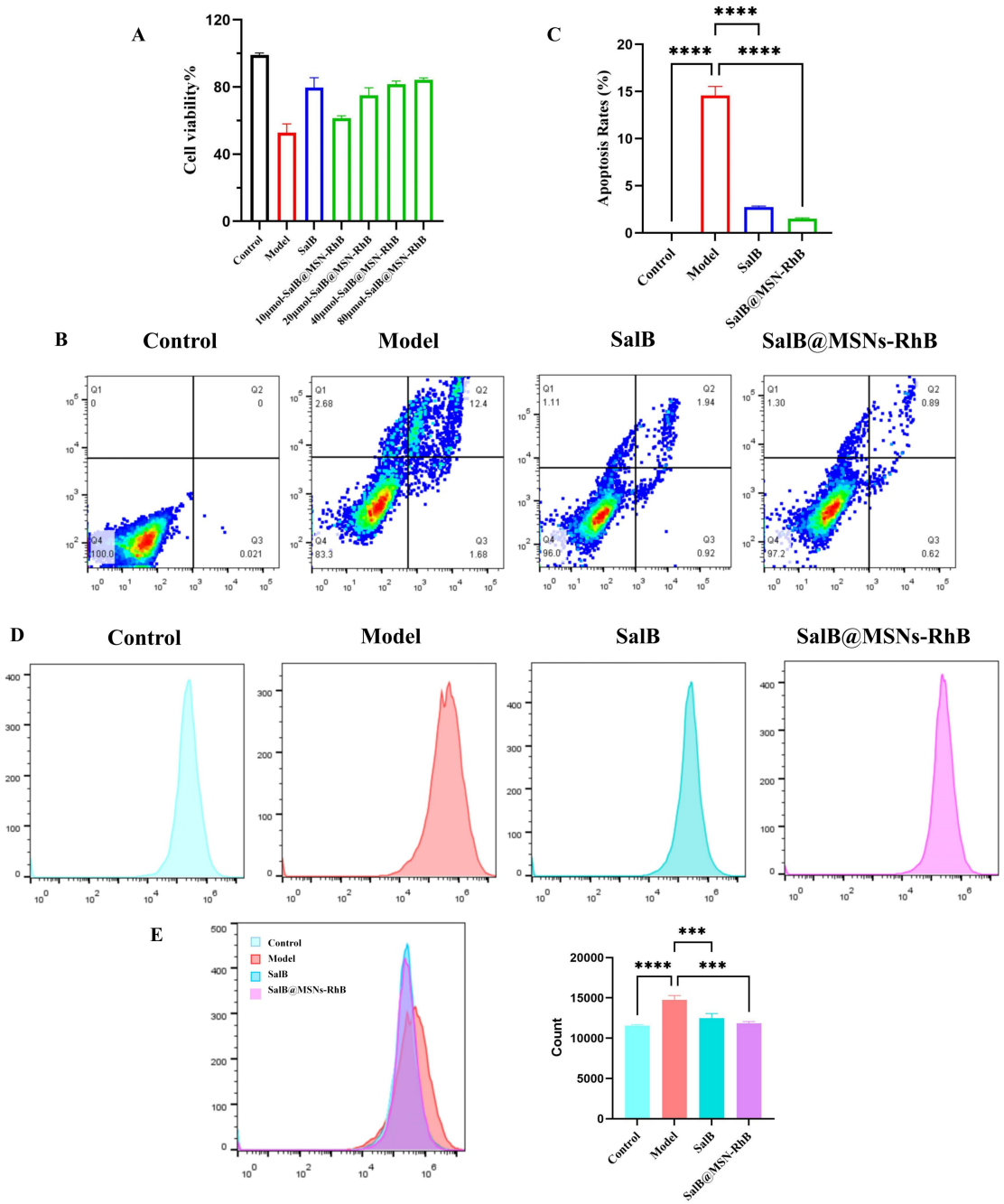

Figure 4 Cell viability, apoptosis and ROS. (A) Effects of SalB@MSNs-RhB, SalB and hypoxia/reoxygenation injury on the growth and viability of normal H9C2 cardiomyocytes. (B) Determination of apoptosis of cells in each group using Annexin V/PI staining. (C) Quantification of apoptotic cells in each group. (D) The levels of ROS in H9C2 cardiomyocytes in each group. (E) Quantification of the levels of ROS in H9C2 cardiomyocytes in each group. * $P < 0.05$, ** $P < 0.01$, *** $P < 0.001$, **** $P < 0.0001$. SalB, salvianolic acid B; MSNs, mesoporous silica nanoparticles; RhB, rhodamine B; ROS, reactive oxygen species.

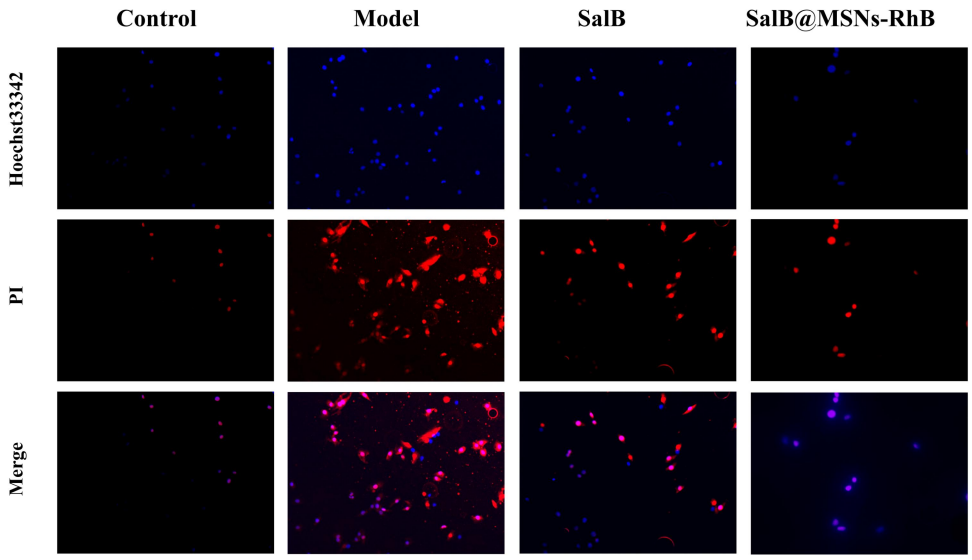

Figure 5 Detection of the nuclei of H9C2 cardiomyocytes in every group under a fluorescence microscope after staining with two days, Hoechst 33342 and PI. PI, propidium iodide.

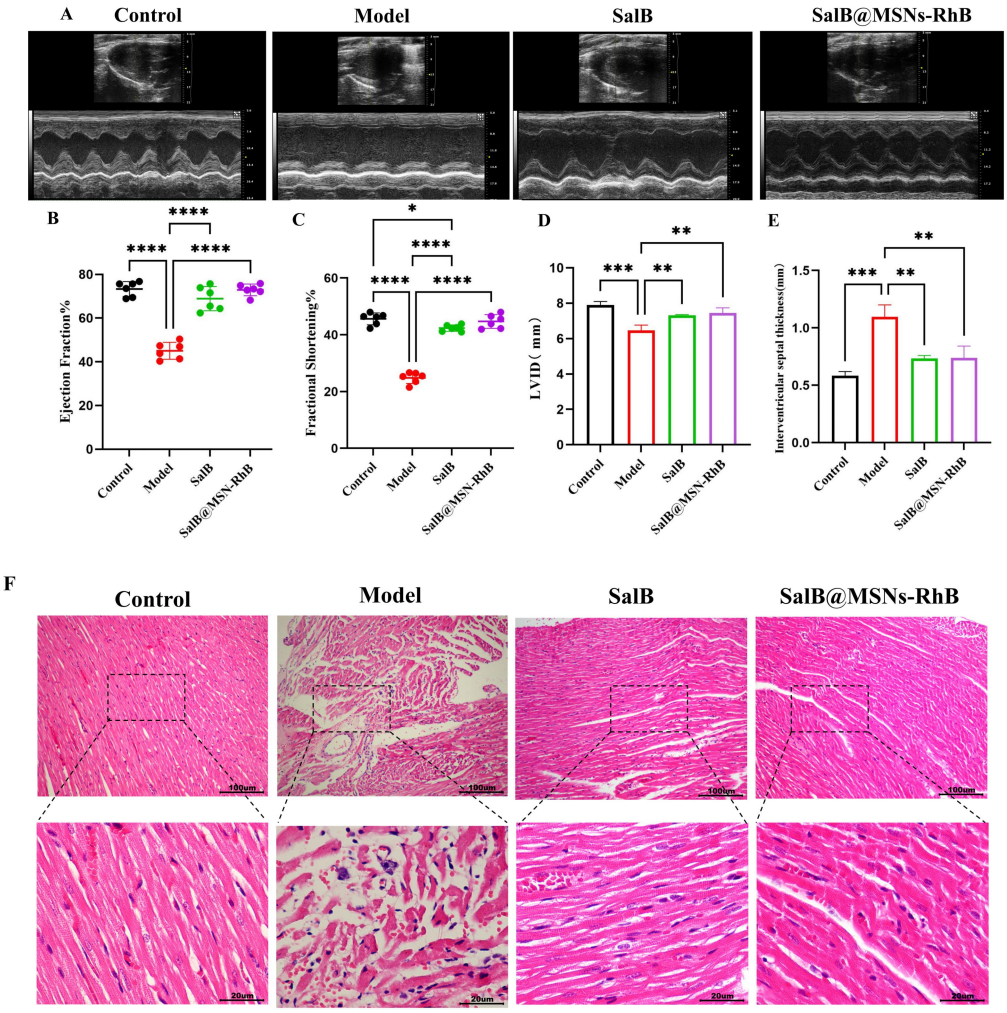

Figure 6 Effects of administration on cardiac function in rats with H/R myocardial injury. (A) Representative echocardiograms from each group. (B) LVEF. (C) LVFS. (D) Left ventricular internal dimension. (E) Interventricular septal thickness. (F) Micrograph depicting hematoxylin and eosin stained heart tissue. * $P < 0.05$, ** $P < 0.01$, *** $P < 0.001$, **** $P < 0.0001$. SalB, salvianolic acid B; MSNs, mesoporous silica nanoparticles; RhB, rhodamine B; LVEF, left ventricular ejection fraction; LVFS, left ventricular fractional shortening.

model was successfully constructed. After SalB@MSNs-RhB treatment, the EF and FS levels increased by 27% and 20%, respectively. Thus, SalB was less effective than SalB@MSNs-RhB.

Pathological changes in the LV of H/R rats were revealed by HE staining. In the model group, LV cardiomyocytes were hypertrophic and disordered. Myocardial cytoplasmic swelling and intercellular widening were also observed. The SalB and SalB-MSN-RhB groups exhibited fewer tissue lesions.

TUNEL immunofluorescence

Figure 7 shows apoptosis in rat myocardial tissue, as measured by TUNEL staining. Compared with the control group, the number of TUNEL positive cells was greater in the model group. Following SalB@MSNs-RhB treatment, the number of TUNEL-positive cells decreased. These results confirm that SalB@MSNs-RhB play an anti-apoptotic role in H/R rats.

Serum biomarkers

To assess the cardioprotective effect of SalB@MSNs-RhB in H/R rats, we measured serum biomarker levels. The H/R model group exhibited markedly elevated serum aspartate transaminase, alanine aminotransferase, malondialdehyde, creatine kinase isoenzyme-MB, lactate dehydrogenase and caspase-3 levels (Figure 8). However, pretreatment with SalB@MSNs-RhB significantly reduced these levels and increased serum superoxide dismutase levels, indicating that SalB@MSNs-RhB attenuated H/R-induced tissue injury in vivo.

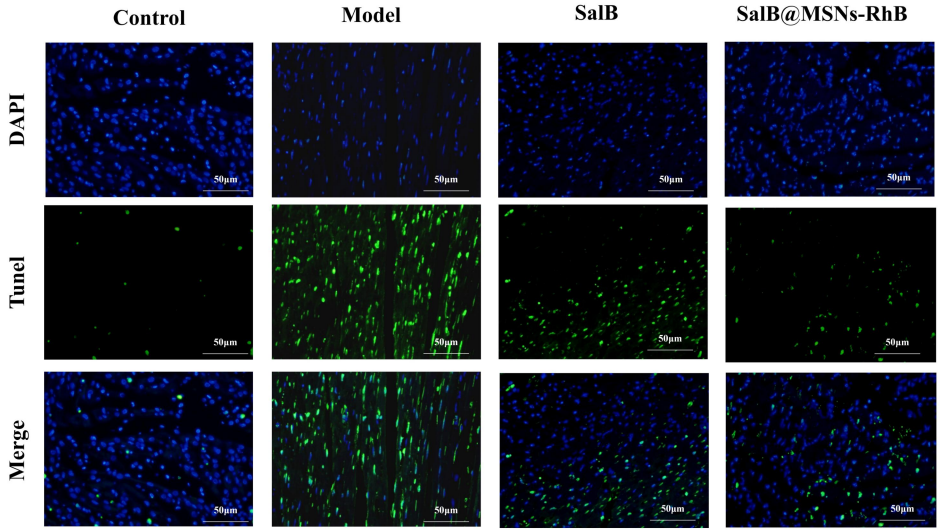

Figure 7 Tunel immunofluorescence staining of rat heart tissue with I/R injury after SalB@MSNs-RhB treatment. Apoptotic cells appeared a bright green under the fluorescence microscope. SalB, salvianolic acid B; MSNs, mesoporous silica nanoparticles; RhB, rhodamine B; I/R, ischemia-reperfusion.

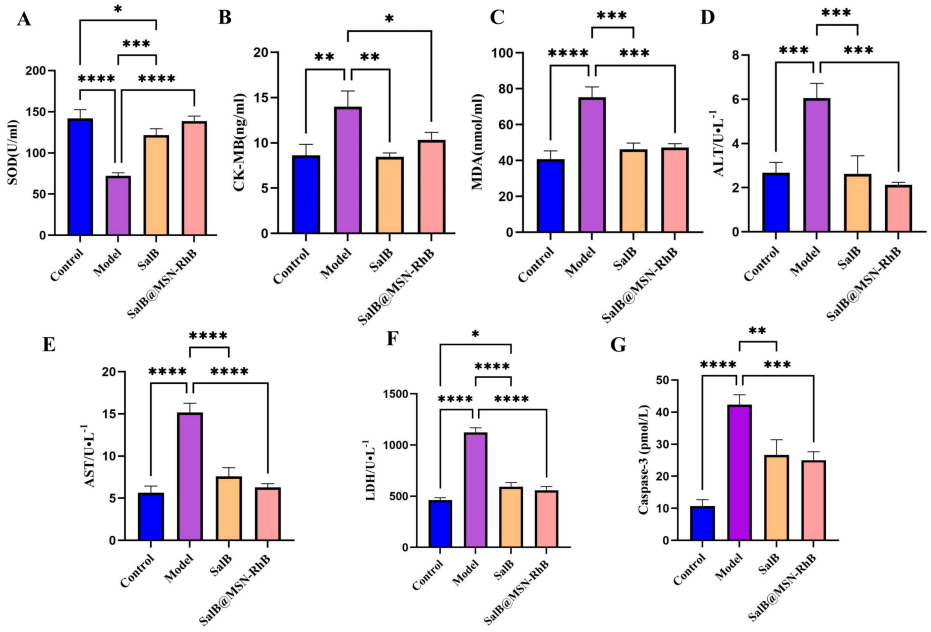

Figure 8 Determination of biochemical indicators. The level of SOD was significantly higher in the SalB and SalB@MSNs-RhB rats than in the model rats. (B) Effect of SalB and SalB@MSNs-RhB on serum CK-MB levels. (C) Effects of SalB and SalB@MSNs-RhB on serum levels of MDA. (D, E) Effects of SalB and SalB@MSNs-RhB on serum levels of ALT and AST. (G) Effect of SalB and SalB@MSNs-RhB on serum levels of caspase-3. *P < 0.05, ** P < 0.01, *** P < 0.001, **** P < 0.0001. SalB, salvianolic acid B; MSNs, mesoporous silica nanoparticles; RhB, rhodamine B; SOD, superoxide dismutase; MDA, malondialdehyde; CK-MB, creatine kinase isoenzyme-MB; ALT, alanine aminotransferase; AST, aspartate transaminase.

Effect of SalB@MSNs-RhB on myocardial-associated proteins in ischemia-reperfused rats

Western blotting was used to investigate the molecular mechanisms underlying the cardioprotective effects of SalB@MSNs-RhB. We analyzed Bax, Bcl-2, and caspase-3 expression in cardiomyocytes using western blotting and investigated the cardiac JAK2/STAT3 signaling pathway. In contrast to the control group, the model group's Bax and caspase-3 protein expression was significantly upregulated ($P < 0.0001$), and its Bcl-2 expression was substantially downregulated (Figure 9A, 9E). A significant reduction in caspase-3 and Bax levels and an increase in Bcl-2 levels were observed during SalB@MSNs-RhB-induced apoptosis (Figure 9C, 9G and 9F). Additionally, the expression of JAK2 and STAT3 substantially increased after SalB@MSNs-RhB administration (Figure 9B, 9D). These results confirmed that SalB@MSNs-RhB inhibited apoptosis by activating the JAK2/STAT3 signaling pathway.

Discussion

The high clinical morbidity and mortality of acute myocardial infarction is a risk to human life and health. Hemodynamic reconstitution therapy (such as, pharmacological thrombolysis, intervention, and bypass) is the primary treatment for acute infarction, effectively reducing patient mortality [26, 27]. However, hemodynamic reconstruction inevitably causes I/R injury, leading to severe myocardial cell death, increased tissue damage, acute and chronic heart failure, and death. The pathogenesis of cardiac I/R injury is complex, and its source-initiating factors and underlying pathogenesis remain unclear [28, 29]. This limits the development of specific targeted therapeutic agents. Currently, no drugs specifically attenuate clinical cardiac I/R injury or the prognosis of hemodialysis.

Salviae Miltiorrhizae Radix et Rhizoma, a herbal medicine extensively used in the treatment of CVD, contains a variety of chemical complexes with a wide range of biological activities, and is a research hotspot in Chinese medicine both within and outside the country [30]. SalB is one of its main active components, which exhibits protective effects on various organs such as the heart, brain, liver, lung, and kidney [31]. However, it has poor stability and low bioavailability [32]. Hence, its preparation and clinical application have become a research hotspot in recent years. Translating theoretical research into practical clinical applications is a common problem that needs to be addressed. The above-mentioned disadvantages of SalB need to be resolved from a formulation point of view, and a suitable carrier for drug delivery systems needs to be identified. MSNs have many unique advantages as carriers in drug delivery systems. First, MSNs have a large specific surface area, such that more drugs can be loaded on the I/R surface or inside the nanopore channel, and they are non-toxic, biocompatible, and recyclable, making them appropriate for clinical diagnostic and therapeutic applications [33, 34].

We developed an ischemia–reperfusion male rat model and H/R cardiomyocytes to study myocardial I/R in this study [35, 36]. SalB@MSNs-RhB were administered to cells and rats to study the improvement of SalB delivery by MSNs and the regulatory mechanism of SalB@MSNs-RhB in affecting I/R on myocardial injury in rats. This, combined with the analysis of in vitro drug release results, we identified that the slower release of SalB loaded into MSNs-RhB contributed to enhanced effective action of SalB in the organism. In addition, according to the cellular activity assay results, 80 μmol of SalB-loaded nanoparticles showed the strongest effect on cellular activity. Therefore, this study investigated the effect of 80 μmol SalB@MSNs-RhB on I/R.

The Bcl-2 family is a vital regulator of endogenous mitochondrial pathway of apoptosis [37, 38]. Bcl-2 and Bax are the main constituents of the Bcl-2 family, the proteins involved in apoptosis and important indicators of myocardial viability [39–41]. Bcl-2 is an apoptosis-inhibiting protein. Bax is a pro-apoptotic protein. Caspase-3 is the executor of apoptosis. Under normal conditions, caspase-3 occurs in the cytoplasm in the form of zymogen and is inactive, getting activated in the early stages of apoptosis onset to cleave cytoplasmic and cytosolic substrates, and initiate apoptosis [42–45]. Results of the present study showed that rat myocardial tissues expressed caspase-3, Bcl-2, and Bax proteins relative to each other within the model group and beyond the control group ($P < 0.05$), confirming that all these apoptotic proteins were abnormally expressed in H/R. After treatment with SalB and SalB@MSNs-RhB, myocardial tissues showed increased Bcl-2 levels and decreased caspase-3 and Bax levels, suggesting that SalB and SalB@MSNs-RhB inhibited apoptosis by inhibiting caspase-3 and Bax and upregulating Bcl-2 to inhibit apoptosis. Although SalB has potent anti-apoptotic effects, its poor stability and low bioavailability limit its uptake and release in living organisms. This study determined that the porous structure of MSNs effectively loaded SalB for uptake and released it into cardiomyocytes by influencing SalB uptake and release.

This study showed that MSNs loaded with SalB resulted in enhanced uptake and release of SalB by cardiomyocytes due to the porous shape of I/R. A significant improvement in the therapeutic effect of SalB was also observed (Figure 10) [46–54].

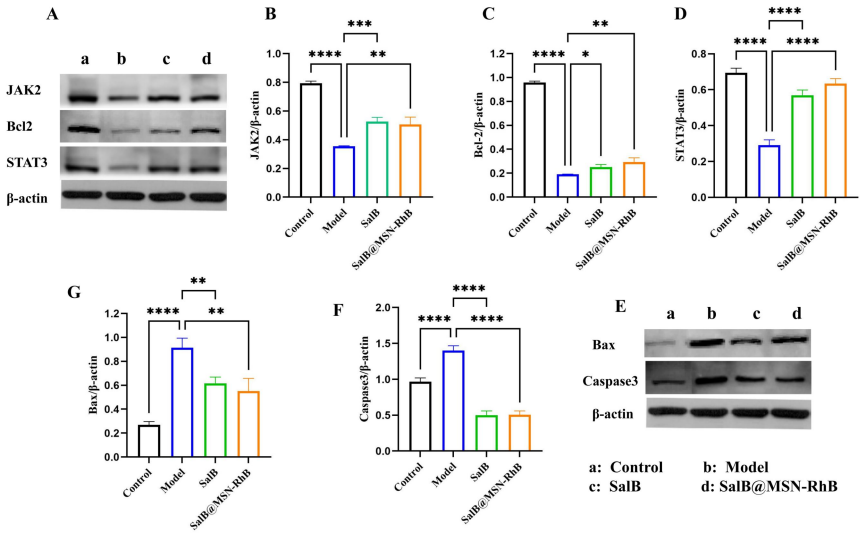

Figure 9 JAK2/STAT3 signaling pathway related proteins. The amount of JAK2, Bcl-2 and STAT3 from heart lysate as examined by western blot analysis. (B–D) Relative protein levels measured by densitometry for JAK2, Bcl-2, and STAT3. (E) The amount of Bax and Caspase 3 from heart lysate examined by western blot analysis. (F, G) Relative protein levels measured by densitometry for Bax and Caspase 3. *$P < 0.05$, ** $P < 0.01$, *** $P < 0.001$, **** $P < 0.0001$. SalB, salvianolic acid B; MSNs, mesoporous silica nanoparticles; RhB, rhodamine B.

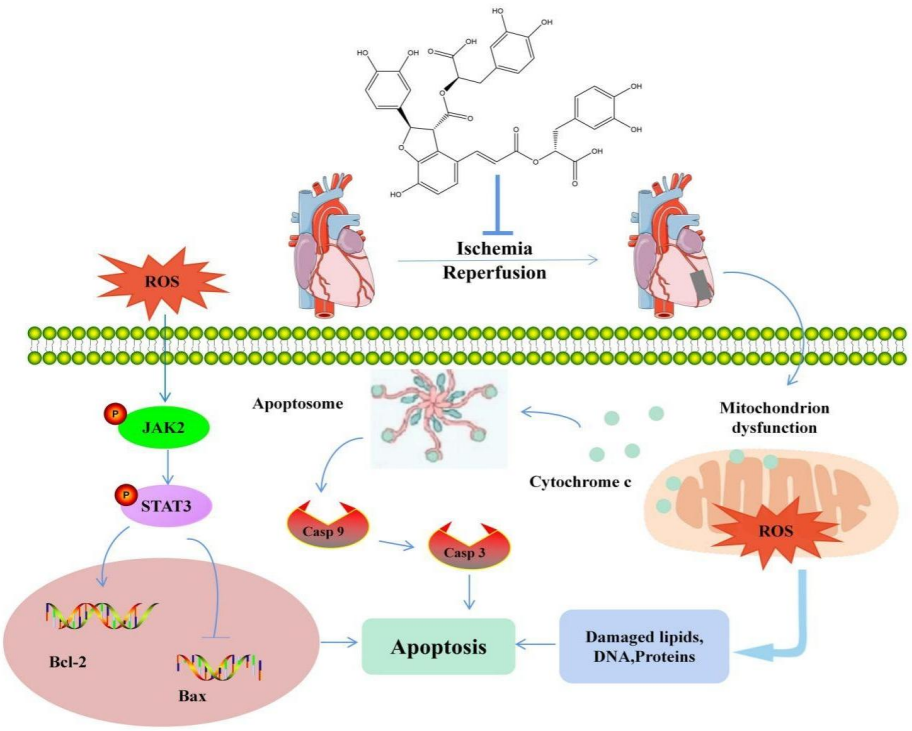

Figure 10 Ischemia-reperfusion mechanism. Increased oxidative stress in vivo aggravates myocardial injury, and increased intracellular ROS accumulation causes mitochondrial dysfunction, further aggravating myocardial apoptosis . ROS generated during oxidative stress may attack polyunsaturated fatty acids within the cell membrane and release lipid peroxides such as MDA. MDA is a biomarker of oxidative stress. LDH release is a common marker of cardiomyocyte injury. Cardiomyocyte injury was assessed by measuring LDH released into the culture medium. In our study, ROS, MDA, and LDH production increased in cardiomyocytes undergoing H/R injury, and SalB@MSNs-RhB treatment reversed these changes. JAK2/STAT3 signaling is a significant transduction pathway involved in various pathological processes, such as oxidative stress, apoptosis, inflammation, and immunity. Upon activation of JAK2/STAT3 signaling, first cells activated JAK2, further phosphorylating STAT3 and transducing extracellular signals to the nucleus, regulating the expression of target genes and exerting biological effects. In our study, the expressions of JAK2 and STAT3 were significantly downregulated in cardiomyocytes subjected to H/R injury, and SalB@MSNs-RhB treatment reversed these changes. SalB, salvianolic acid B; MSNs, mesoporous silica nanoparticles; RhB, rhodamine B; ROS, reactive oxygen species; MDA, malondialdehyde; LDH, lactate dehydrogenase.

Conclusion

Taken together, SalB and SalB@MSNs-RhB have protective effects on cardiac function in rats with myocardial I/R injury. The I/R mechanisms of action may be associated with the reduction of oxidative stress and inhibition of cellular regulation. Our results demonstrated that SalB@MSNs-RhB improved the bioavailability and therapeutic effects of SalB, enhancing JAK2/STAT3-dependent pro-survival signaling and antioxidant responses, thereby protecting cardiomyocytes from I/R injury-induced oxidative stress and apoptosis. These results provide foundational information for accelerating the development of SalB as a clinical therapeutic agent for CVD and offer new insights into therapeutic strategies for myocardial I/R injury.

References

1. Pagliaro BR, Cannata F, Stefanini GG, Bolognese L. Myocardial ischemia and coronary disease in heart failure. *Heart Fail Rev* 2020;25(1):53–65. Available at: http://doi.org/10.1007/s10741-019-09831-z
2. Wu Y, Liu H, Wang X. Cardioprotection of pharmacological postconditioning on myocardial ischemia/reperfusion injury. *Life Sci* 2021;264:118628. Available at: http://doi.org/10.1016/j.lfs.2020.118628
3. Heusch G. Myocardial ischaemia–reperfusion injury and cardioprotection in perspective. *Nat Rev Cardiol* 2020;17(12):773–789. Available at: http://doi.org/10.1038/s41569-020-0403-y
4. Wu MY, Yiang GT, Liao WT, et al. Current Mechanistic Concepts in Ischemia and Reperfusion Injury. *Cell Physiol Biochem* 2018;46(4):1650–1667. Available at: http://doi.org/10.1159/000489241
5. Cadenas S. ROS and redox signaling in myocardial ischemia-reperfusion injury and cardioprotection. *Free Radical Biol Med* 2018;117:76–89. Available at: http://doi.org/10.1016/j.freeradbiomed.2018.01.024
6. Yao J. W. A brief discussion on the side effects of Western Medicine and its targeted Relief methods[J]. *J Clin Med* 2017, 4(95):18764-18765＋18768. Available at: http://doi.org/10.16281/j.cnki.jocml.2017.95.124.
7. Ho J, Hong CY. Salvianolic acids: small compounds with multiple mechanisms for cardiovascular protection. *J Biomed Sci* 2011;18(1):30. Available at: http://doi.org/10.1186/1423-0127-18-30
8. Joe Y, Zheng M, Kim HJ, et al. Salvianolic Acid B Exerts Vasoprotective Effects through the Modulation of Heme Oxygenase-1 and Arginase Activities. *J Pharmacol Exp Ther* 2012;341(3):850–858. Available at: http://doi.org/10.1124/jpet.111.190736
9. Xiao SL, Ding SL, Sun ZX, Liao FL, You Y. [Platelet function tests and Chinese medicines with antiplatelet function:a review]. *Zhongguo Zhong Yao Za Zhi* 2021, 46 (19), 4907-4921. Available at: http://doi.org/10.19540/j.cnki.cjcmm.20210618.701
10. Cao W, Guo X, Zheng H, Li D, Jia G, Wang J. Current progress of research on pharmacologic actions of salvianolic acid B. *Chin J Integr Med* 2012;18(4):316–320. Available at:

http://doi.org/10.1007/s11655-012-1052-8
11. Xiao Z, Liu W, Mu Y, et al. Pharmacological Effects of Salvianolic Acid B Against Oxidative Damage. *Front Pharmacol* 2020;11. Available at: http://doi.org/10.3389/fphar.2020.572373
12. Li Y, Liu Y, Yan X, Liu Q, Zhao YH, Wang DW. Pharmacological Effects and Mechanisms of Chinese Medicines Modulating NLRP3 Inflammasomes in Ischemic Cardio/Cerebral Vascular Disease. *Am J Chin Med* 2018;46(08):1727–1741. Available at: http://doi.org/10.1142/S0192415X18500878
13. Yu LJ, Zhang KJ, Zhu JZ, et al. Salvianolic Acid Exerts Cardioprotection through Promoting Angiogenesis in Animal Models of Acute Myocardial Infarction: Preclinical Evidence. *Oxid Med Cell Longev* 2017;2017:8192383. Available at: http://doi.org/10.1155/2017/8192383
14. Li ZY, Li ZH, He JH, Liu JP. Pellets of Phospholipids and D-Glucose with Improved Intestinal Absorption and Oral Bioavailability of Salvianolic Acid B. *Pharm. Dev. Technol* 2022;27(2):190–201. Available at: http://doi.org/10.1080/10837450.2022.2033998
15. Ahmad N, Ahmad R, Ahmad FJ, et al. Poloxamer-chitosan-based Naringenin nanoformulation used in brain targeting for the treatment of cerebral ischemia. *Saudi J Biol Sci* 2020;27(1):500–517. Available at: http://doi.org/10.1016/j.sjbs.2019.11.008
16. Ugazio E, Gastaldi L, Brunella V, et al. Thermoresponsive mesoporous silica nanoparticles as a carrier for skin delivery of quercetin. *Int J Pharm* 2016;511(1):446–454. Available at: http://doi.org/10.1016/j.ijpharm.2016.07.024
17. Sapino S, Ugazio E, Gastaldi L, et al. Mesoporous silica as topical nanocarriers for quercetin: characterization and in vitro studies. *Eur J Pharm Biopharm* 2015;89:116–125. Available at: http://doi.org/10.1016/j.ejpb.2014.11.022
18. Zhao T, Wu W, Sui L, et al. Reactive oxygen species-based nanomaterials for the treatment of myocardial ischemia reperfusion injuries. *Bioact Mater* 2022;7:47–72. Available at: http://doi.org/10.1016/j.bioactmat.2021.06.006
19. Teng W, Yang Z, Wang S, Xiong D, Chen Y, Wu Z. Toxicity evaluation of mesoporous silica particles Santa Barbara No. 15 amorphous in human umbilical vein endothelial cells: influence of particle morphology. *J Appl Toxicol* 2021;41 (9):1467-1478. Available at: http://doi.org/10.1002/jat.4137
20. Cuello NI, Elías VR, Mendieta SN, et al. Drug release profiles of modified MCM-41 with superparamagnetic behavior correlated with the employed synthesis method. *Mater Sci Eng C Mater Biol Appl* 2017;78:674–681. Available at: http://doi.org/10.1016/j.msec.2017.02.010
21. Horcajada P, Márquez-Alvarez C, Rámila A, Pérez-Pariente J, Vallet-Regí M. Controlled release of Ibuprofen from dealuminated faujasites. *Solid State Sci* 2006;8(12):1459–1465. Available at: http://doi.org/10.1016/j.solidstatesciences.2006.07.016
22. Andersson J, Rosenholm J, Areva S, Lindén M. Influences of Material Characteristics on Ibuprofen Drug Loading and Release Profiles from Ordered Micro- and Mesoporous Silica Matrices. *Chem Mater* 2004;16(21):4160–4167. Available at: http://doi.org/10.1021/cm0401490
23. Zhu Y, Shi J, Li Y, Chen H, Shen W, Dong X. Storage and release of ibuprofen drug molecules in hollow mesoporous silica spheres with modified pore surface. *Microporous Mesoporous Mater* 2005;85(1–2):75–81. Available at: http://doi.org/10.1016/j.micromeso.2005.06.015
24. Cooksey C. Quirks of dye nomenclature. 5. Rhodamines. *Biotech Histochem* 2015;91 (1):71–76. Available at: http://doi.org/10.3109/10520295.2015.1074287
25. Kim HN, Lee MH, Kim HJ, Kim JS, Yoon J. A new trend in rhodamine-based chemosensors: application of spirolactam ring-opening to sensing ions. *Chem Soc Rev* 2008;37(8):1465. Available at: http://doi.org/10.1039/b802497a
26. Gerbaud E, Elbaz M, Lattuca B. New insights into cardiogenic shock and coronary revascularization after acute myocardial infarction. *Arch Cardiovasc Dis* 2020;113(4):276–284. Available at: http://doi.org/10.1016/j.acvd.2019.12.005
27. Rout A, Tantry US, Novakovic M, Sukhi A, Gurbel PA. Targeted pharmacotherapy for ischemia reperfusion injury in acute myocardial infarction. *Expert Opin Pharmacother* 2020;21(15):1851–1865. Available at: http://doi.org/10.1080/14656566.2020.1787987
28. Yan HF, Tuo QZ, Yin QZ, Lei P. The pathological role of ferroptosis in ischemia/reperfusion-related injury. *Zool Res* 2020;41(3):220–230. Available at: http://doi.org/10.24272/j.issn.2095-8137.2020.042
29. Li XY, Ma N, Xu JP, et al. Targeting Ferroptosis: Pathological Mechanism and Treatment of Ischemia-Reperfusion Injury. *Oxid Med and Cell Longev* 2021;2021:1587922. Available at: http://doi.org/10.1155/2021/1587922
30. Shi M, Huang F, Deng C, Wang Y, Kai G. Bioactivities, biosynthesis and biotechnological production of phenolic acids in Salvia miltiorrhiza. *Crit Rev Food Sci Nutr* 2018;59(6):953–964. Available at: http://doi.org/10.1080/10408398.2018.1474170
31. Wu Y, Xu S, Tian XY. The Effect of Salvianolic Acid on Vascular Protection and Possible Mechanisms. *Oxid Med Cell Longev* 2020;2020:1–9. Available at: http://doi.org/10.1155/2020/5472096
32. Li ZY, Li ZH, He JH, Liu JP. Pellets of Phospholipids and D-Glucose with Improved Intestinal Absorption and Oral Bioavailability of Salvianolic Acid B. *Pharm. Dev. Technol* 2022;27(2):190–201. Available at: http://doi.org/10.1080/10837450.2022.2033998
33. Pu X, Li J, Qiao P, et al. Mesoporous Silica Nanoparticles as a Prospective and Promising Approach for Drug Delivery and Biomedical Applications. *Curr Cancer Drug Targets* 2019;19(4):285–295. Available at: http://doi.org/10.2174/1568009619666181206114904
34. Zang X, Zhou J, Zhang X, Han Y, Chen X. Ischemia Reperfusion Injury: Opportunities for Nanoparticles. *ACS Biomater Sci Eng* 2020;6(12):6528–6539. Available at: http://doi.org/10.1021/acsbiomaterials.0c01197
35. Song N, Yang YW. Molecular and supramolecular switches on mesoporous silica nanoparticles. *Chem Soc Rev* 2015;44(11):3474–3504. Available at: http://doi.org/10.1039/C5CS00243E
36. Bilia A, Piazzini V, Guccione C, et al. Improving on Nature: The Role of Nanomedicine in the Development of Clinical Natural Drugs. *Planta Med* 2017;83(05):366–381. Available at: http://doi.org/10.1055/s-0043-102949
37. Liu XM, Yang ZM, Liu XK. Fas/FasL Induces Myocardial Cell Apoptosis in Myocardial Ischemia-Reperfusion Rat Model. *Eur. Rev. Med. Pharmacol. Sci* 2017, 21 (12), 2913–2918. Available at: https://pubmed.ncbi.nlm.nih.gov/28682425/
38. Liu X, Zhang S, Xu C, et al. The Protective of Baicalin on Myocardial Ischemia-Reperfusion Injury. *Curr Pharm Biotechnol* 2020;21(13):1386–1393. Available at: http://doi.org/10.2174/1389201021666200605104540
39. Zhang Y, Yang X, Ge X, Zhang F. Puerarin attenuates neurological deficits via Bcl-2/Bax/cleaved caspase-3 and Sirt3/SOD2 apoptotic pathways in subarachnoid hemorrhage mice. *Biomed Pharmacother* 2019;109:726–733. Available at: http://doi.org/10.1016/j.biopha.2018.10.161
40. Korshunova A, Blagonravov M, Neborak E, et al. BCL2-regulated apoptotic process in myocardial ischemia-reperfusion injury (Review). *Int J Mol Med* 2020;47(1):23–36. Available at: http://doi.org/10.3892/ijmm.2020.4781
41. Chipuk JE, Fisher JC, Dillon CP, Kriwacki RW, Kuwana T, Green

DR. Mechanism of apoptosis induction by inhibition of the anti-apoptotic BCL-2 proteins. *Proc Natl Acad Sci USA* 2008;105(51):20327–20332. Available at: http://doi.org/10.1073/pnas.0808036105

42. Senichkin VV, Pervushin NV, Zuev AP, Zhivotovsky B, Kopeina GS. Targeting Bcl-2 Family Proteins: What, Where, When? *Biochemistry (Mosc)* 2020;85 (10):1210–1226. Available at: http://doi.org/10.1134/S0006297920100090
43. Banjara S, Suraweera CD, Hinds MG, Kvansakul M. The Bcl-2 Family: Ancient Origins, Conserved Structures, and Divergent Mechanisms. *Biomolecules* 2020;10(1):128. Available at: http://doi.org/10.3390/biom10010128
44. Li Z, Xiao G, Wang H, He S, Zhu Y. A preparation of Ginkgo biloba L. leaves extract inhibits the apoptosis of hippocampal neurons in post-stroke mice via regulating the expression of Bax/Bcl-2 and Caspase-3. *J Ethnopharmacol* 2021;280:114481. Available at: http://doi.org/10.1016/j.jep.2021.114481
45. Zhang Y, Yang X, Ge X, Zhang F. Puerarin attenuates neurological deficits via Bcl-2/Bax/cleaved caspase-3 and Sirt3/SOD2 apoptotic pathways in subarachnoid hemorrhage mice. *Biomed Pharmacother* 2019;109:726–733. Available at: http://doi.org/10.1016/j.biopha.2018.10.161
46. Lei Q, Huang X, Zheng L, et al. Biosensors for Caspase-3: From chemical methodologies to biomedical applications. *Talanta* 2022;240:123198. Available at: http://doi.org/10.1016/j.talanta.2021.123198
47. Araya LE, Soni IV, Hardy JA, Julien O. Deorphanizing Caspase-3 and Caspase-9 Substrates In and Out of Apoptosis with Deep Substrate Profiling. *ACS Chem Biol* 2021;16(11):2280–2296. Available at: http://doi.org/10.1021/acschembio.1c00456
48. Senoner T, Dichtl W. Oxidative Stress in Cardiovascular Diseases: Still a Therapeutic Target? *Nutrients* 2019;11 (9):2090. Available at: http://doi.org/10.3390/nu11092090
49. Steven S, Frenis K, Oelze M, et al. Vascular Inflammation and Oxidative Stress: Major Triggers for Cardiovascular Disease. *Oxid Med Cell Longev* 2019;2019:7092151. Available at: http://doi.org/10.1155/2019/7092151
50. Daiber A, Steven S, Euler G, Schulz R. Vascular and Cardiac Oxidative Stress and Inflammation as Targets for Cardioprotection. *Curr Pharm Des* 2021;27(18):2112–2130. Available at: http://doi.org/10.2174/1381612827666210125155821
51. Tsikas D, Rothmann S, Schneider JY, et al. Development, Validation and Biomedical Applications of Stable-Isotope Dilution GC-MS and GC-MS/MS Techniques for Circulating Malondialdehyde (MDA) after Pentafluorobenzyl Bromide Derivatization: MDA as a Biomarker of Oxidative Stress and Its Relation to 15(S)-8-Iso-Prostaglandin F2α and Nitric Oxide (NO). *J Chromatogr B Analyt Technol Biomed Life Sci* 2016;1019: 95–111. Available at: http://doi.org/10.1016/j.jchromb.2015.10.009
52. Wang D, Chen T, Liu F. Betulinic acid alleviates myocardial hypoxia/reoxygenation injury via inducing Nrf2/HO-1 and inhibiting p38 and JNK pathways. *Eur J Pharmacol* 2018;838:53–59. Available at: http://doi.org/10.1016/j.ejphar.2018.08.024
53. Zhong Y, Yin B, Ye Y, et al. The bidirectional role of the JAK2/STAT3 signaling pathway and related mechanisms in cerebral ischemia-reperfusion injury. *Exp Neurol* 2021;341: 113690. Available at: http://doi.org/10.1016/j.expneurol.2021.113690
54. Tang Y, Tong X, Li Y, et al. JAK2/STAT3 pathway is involved in the protective effects of epidermal growth factor receptor activation against cerebral ischemia/reperfusion injury in rats. *Neurosci Lett* 2018;662:219–226. Available at: http://doi.org/10.1016/j.neulet.2017.10.037